Fault seal calibration: a brief review

G. YIELDING*, P. BRETAN & B. FREEMAN

Badley Geoscience Limited, North Beck House, North Beck Lane, Hundleby, Spilsby, Lincolnshire, PE23 5NB, UK

**Corresponding author (e-mail: graham@badleys.co.uk)*

Abstract: Calibration is a necessary step in the workflow for prediction of fault seal because there is no direct way to detect the hydraulic behaviour of a fault at the scale of a hydrocarbon trap. Over the last 20 years two general approaches have been developed:

(i) Measurement of hydraulic properties of fault-zone samples (lab calibration), then mapping these results onto the appropriate parts of trap-bounding faults.
(ii) Design of simple algorithms which attempt to capture a salient feature of the fault zone (e.g. CSP, SSF, SGR), then looking at known trap-bounding faults to find a relationship between the algorithm and the presence or capacity of a seal (sub-surface calibration).

Seal capacity is typically described by Hg–air threshold pressure in the lab or static pressure differences in the subsurface (e.g. hydrocarbon buoyancy pressure). In addition to likely interpretation and geometry errors in approaches (i) and (ii), further uncertainty is introduced when converting the calibrated seal strength to potential hydrocarbon column height, because of the variability of subsurface hydrocarbon fluids (interfacial tension). Despite these potential problems, the different methodologies typically agree reasonably well in their predictions for fault-seal capacity. However, this agreement may be largely coincidental and is likely to be a response to the heterogeneity of fault-zone structure (especially at intermediate 'compositions' or SGR).

Faults frequently form the side-seals to hydrocarbon reservoir compartments. Identification of faults as apparent side-seals usually comes from recognition of different hydrocarbon contacts across a fault, from measurement of different reservoir pore-pressures in adjacent compartments, or from poor flow performance in a producing reservoir. Note that all of these techniques relate to fluid behaviour measured in adjacent wells, and not to any measurement of the fault itself. In essence, this is the fault seal 'problem' – we cannot directly image the sealing properties of fault zones using seismic reflection data (though direct hydrocarbon indicators such as flat spots may locally help). So instead, we must find something we *can* measure, and then relate that proxy property to the known geological processes that may cause a fault to seal. The act of checking the predictions at known sealing faults is the process of 'fault seal calibration'.

Before proceeding further, it is worth clarifying the word 'seal'. A dictionary definition (Oxford Paperback Dictionary 1988) is 'a substance used to close an opening and prevent air or liquid from flowing through it'. This is the context in which the word is used in exploration and appraisal – we are looking for a lithological seal that has prevented hydrocarbon flow on a geological time-scale, so that a commercial accumulation is still present when the trap is drilled. However, in a production/development context, the term 'sealing fault' is often used for a fault that acts as an impairment or baffle to flow on a production time-scale, rather than something that completely prevents flow. The influence of a baffle on flow is dependent upon its permeability and thickness, whereas the static trapping capability is mainly dependent upon the capillary properties (see below). In this contribution, we shall focus on the exploration definition, that is, a seal as a lithology or structure that can hold a hydrocarbon column in place over a geological time-scale.

How do faults seal?

There are three fundamental conditions which control the sealing behaviour of a fault in siliciclastic sequences (see Fig. 1):

(1) The juxtaposition of the reservoir against sealing lithologies across the fault.
(2) Fault-zone products created by deformation during the fault displacement and subsequent evolution.
(3) The current stress state of the fault and its proximity to failure (slip).

The first condition is geometric, and provides a way for a shale (or other sealing lithology) to be

From: JOLLEY, S. J., FISHER, Q. J., AINSWORTH, R. B., VROLIJK, P. J. & DELISLE, S. (eds) *Reservoir Compartmentalization*. Geological Society, London, Special Publications, **347**, 243–255.
DOI: 10.1144/SP347.14 0305-8719/10/$15.00

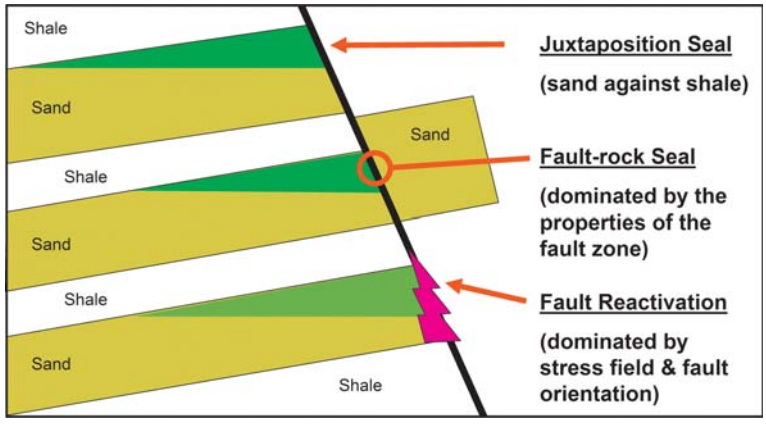

Fig. 1. Cartoon to illustrate the three critical factors for a viable fault seal: juxtaposition seal, fault rock seal, and *in-situ* stress state.

placed in a position where it can be a side-seal to a reservoir compartment. Accurate subsurface mapping of the fault system is critical to assessment of juxtaposition geometries, or as Tearpock & Bishke (2003) succinctly state, 'If you want to drill more than your share of dry holes, don't map faults'. Jolley *et al.* (2007) provide a powerful example of how simple errors in the fault-network geometry can render a subsurface model useless in terms of its flow properties. Although across-fault juxtaposition relationships have traditionally been assessed using fault-plane maps or Allan diagrams (Allan 1989), a true 3D approach is increasingly employed to represent the 3D topology of potential reservoir connections and separations (e.g. Dee *et al.* 2005).

In places where reservoir–reservoir juxtaposition occurs at the fault, it is possible that the fault zone itself can provide the necessary conditions for a side-seal. Most fault-zone rocks have capillary threshold pressures significantly larger than reservoir rocks (e.g. Fisher & Knipe 2001; Sperrevik *et al.* 2002). The fault-zone rock-type depends upon the composition of the faulted sequence, and the burial/temperature history during and after faulting. We discuss these aspects in more detail below.

The third condition describes the *in-situ* stress state of the fault zone. Barton *et al.* (1995) present compelling evidence that in low-permeability host rocks the permeability of a fracture surface is controlled by the stress state – fractures are only permeable when critically stressed, that is, close to failure. Hence a critically-stressed fault may act as leak zone through the reservoir overburden.

It is important to note that a critical stress state is a vertical leakage criterion, not a seal criterion: if a fault is not critically stressed then this tells us nothing about whether it may be a side-seal to a compartment. The juxtaposition geometry and/or fault-zone properties are required to set up the seal. So the three conditions illustrated in Figure 1 may be summarized as (Jones & Hillis 2003): A fault is sealing:

- IF the reservoir is juxtaposed against a sealing lithology,
- OR fault rock provides a seal,
- AND the fault is not critically stressed.

The rest of this paper is concerned principally with the second of these three sealing conditions.

Fault-zone processes

In this section we very briefly review the formation of fault rock in siliciclastic reservoir sequences. The main factors influencing the nature of the deformation products found in fault zones are:

- The composition and rheology of the wall-rocks that are slipping past each other at the fault, in particular their content of fine-grained phyllosilicate clay minerals.
- The stress conditions at the time of faulting, which are most strongly controlled by the tectonic setting and the initial depth of burial during faulting.
- The maximum temperature experienced by the fault zone after faulting, controlled by the maximum post-faulting burial depth and the geothermal gradient.

Figure 2 provides examples of the typical fault rocks produced by different combinations of the first two factors (plotted schematically on the horizontal and vertical axes respectively).

When the wall-rocks contain significant beds of clay or shale, then clay smears or shale smears can be produced down the fault plane, depending on the burial depth and degree of consolidation of the

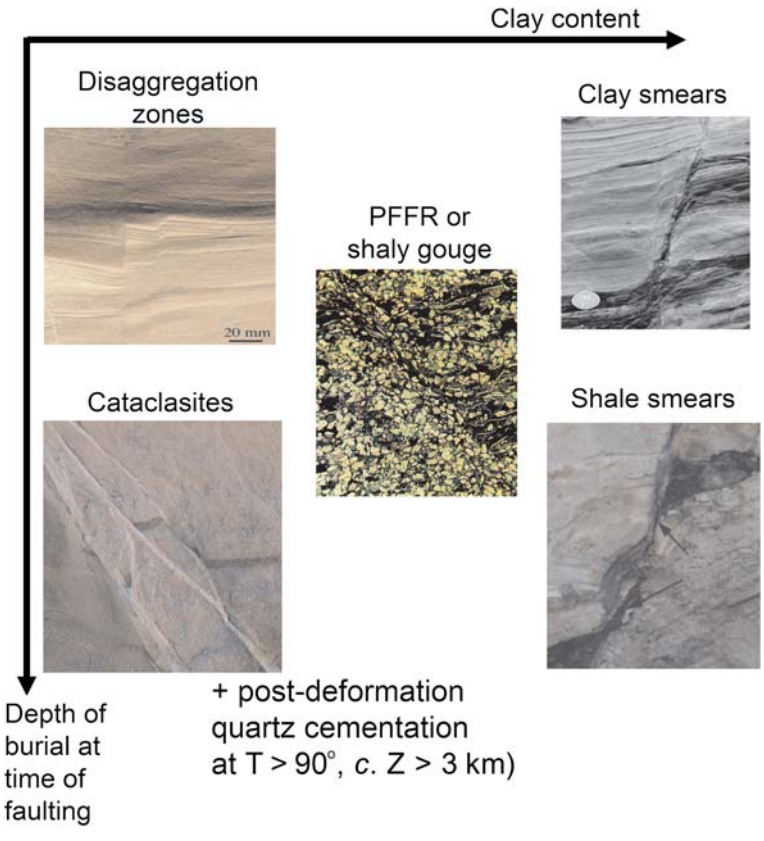

Fig. 2. Schematic plot to illustrate the main fault rock types generated in siliciclastic sequences. The axes represent 2 of the 3 main controls (clay content, and stress conditions during faulting); the third main control is post-faulting temperature history. Photographs from Lindsay *et al.* (1993), Fristad *et al.* (1997), Fossen & Gabrielsen (2005), van der Zee & Urai (2005), Fossen *et al.* (2007).

beds. Clay smears represent a ductile deformation, and are often wedge-shaped with the thickest smear immediately adjacent to the source bed (e.g. Weber *et al.* 1978; Lehner & Pilaar 1997; Aydin & Eyal 2002; van der Zee & Urai 2005; Eichhubl *et al.* 2005). Penetration of such features in the subsurface demonstrates their ability to sustain differences in fluid type and pore-pressure (e.g. Færseth 2006). In cases where the sequence was more deeply buried and lithified during faulting, shale smears can be generated by abrasion rather than ductile flow, producing thin shale veneers of approximately constant thickness along the fault plane (Lindsay *et al.* 1993). Both clay smears and shale smears tend to become disrupted with increasing fault displacement: disruption can occur at any point in the smear but is often near the upthrown or downthrown source bed (Childs *et al.* 2007).

In clay-poor sequences, the principal fault rock types are disaggregation zones and cataclasites (Fisher & Knipe 2001; Sperrevik *et al.* 2002; Fossen & Gabrielsen 2005). Disaggregation zones are formed during fault slip at relatively low confining stress, and are characterized by grain reorganization without grain fracturing. Consequently they tend to have similar hydraulic properties to their host sandstones. At higher effective stress (e.g. burial >1 km) cataclastic processes become significant and the resultant grain fragments infill the pore-space resulting in higher capillary threshold pressure and lower permeability.

Both disaggregation zones and cataclasites are prone to post-deformation quartz cementation if subjected to temperatures $>90\,^{\circ}$C (e.g. Fisher *et al.* 2003), which would be at depths >3 km in typical geothermal gradients. The process of quartz dissolution and re-precipitation might be expected to be more significant in cataclasites because of the greater (and uncoated) surface area of the poorly sorted, comminuted grain fragments.

In sediments of intermediate composition (15–40% phyllosilicate), microfaults are characterized

by a texture termed phyllosilicate-framework fault rock (Fisher & Knipe 1998), or more simply clay-matrix gouge or shaly gouge (e.g. Gibson 1998). Deformation-induced mixing of quartz grains and clay matrix occurs, generally without grain fracturing. With increased burial, both chemical and mechanical compaction may result.

With such a variety of fault rocks, it is clear that the 'sealing capacity of a fault' is not generally a single number, but will vary both along-strike and down-dip on the fault surface. Depending on the disposition of sand-rich or clay-rich beds in the host sequence, and the amount of displacement on the fault, different parts of the fault zone may have very different compositions and fault rocks because of the different beds dragged past each point. Stress conditions during faulting, and temperature history after faulting, are also likely to vary over large (seismically-mappable) fault surfaces. Therefore, to predict the sealing behaviour of the fault we need a methodology to estimate the probable fault-zone composition at each point on the fault surface, and couple this to relevant parameters in the burial (stress/temperature) history.

Fault seal algorithms

Fault seal algorithms are simply a way of automating part of the process of predicting the properties of the fault zone. They fall into 2 broad categories (Yielding *et al.* 1997): smear factors which describe aspects of smearing of clay or shale beds, and gouge ratio which notionally describes the composition of the fault rock.

The Clay Smear Potential (CSP) was developed by Shell in the 1980s (Bouvier *et al.* 1989; Fulljames *et al.* 1997; Lehner & Pilaar 1997). Based on observations of ductile clay smears, and a model of Newtonian viscous flow, the CSP at any point between the two halves of an offset clay bed is dependent on the square of the clay bed thickness and the distance of the point from the nearest half of the bed (Fig. 3). If multiple clay beds are involved then the result is the sum of their contributions. The CSP does not predict the actual thickness of the clay smear, but rather the general likelihood of clay smear to be developed (high CSP = higher likelihood of smear). The relationship gives greater weight to thicker clay beds, and the distance term relates to the tapering of individual clay smear wedges away from the source bed. Doughty (2003) suggests that a thickness exponent of 1.7 rather than 2 gives a better description of clay smears at outcrop for the Calabacillas Fault, New Mexico.

The Shale Smear Factor (SSF) was published by Lindsay *et al.* (1993) following studies of abrasion-type shale smears at outcrop. SSF is simply the ratio of throw to bed thickness for a single offset shale bed (Fig. 3). This ratio is clearly a single number that does not vary up/down the fault plane between the offset halves of the bed, but would vary laterally as fault throw changes. A low SSF corresponds to a higher likelihood of intact smear (see below).

Gouge ratio methods make a simple assumption that the wall rocks are, on average, mixed into the fault zone in a uniform way. Therefore the bulk composition of any part of the fault rock will be the same as the bulk composition of the wall rocks that have slipped past that part of the fault. The key compositional component for sealing potential is the clay content, since small grain sizes lead to small pore-throats and therefore to high capillary threshold pressure. The Shale Gouge Ratio (SGR) algorithm (Yielding *et al.* 1997; Freeman *et al.* 1998) takes the average clay content of those beds that have slipped past any point (as determined by the fault throw), and treats this as an estimate of upscaled fault-zone composition (Fig. 3). Where SGR is high ($>40-50\%$) the fault rock is assumed to be dominated by clay smears, where SGR is low ($<15-20\%$) the fault rock is likely to be disaggregation zone or cataclasites. There is some observational support for this assumption (Yielding 2002; van der Zee & Urai 2005), though there are important scaling issues that are further discussed below.

Figure 4 shows how these fault seal attributes can be mapped onto a fault plane in a subsurface model. The example shows one fault surface, mapped in a 3D seismic survey from offshore Gulf of Mexico. Local well data provide information on the lithological sequence, which can be mapped onto each side of the fault (upthrown Vclay distribution shown at top left). The displacement distribution on the fault is shown at bottom left. Combining these two inputs in the SGR equation (Fig. 3) allows us to plot the variation of SGR over the entire mapped fault surface (Fig. 4, right). In the chosen colour scheme, orange and red indicate SGR $>50\%$ and therefore probably clay smeared, whereas green indicates SGR $<15\%$ and therefore probably disaggregation zone or cataclasite depending on the burial history. Note the lateral and vertical variation in the SGR prediction, and the greater heterogeneity in the results where the fault displacement is low (lateral and upper tip regions).

Calibration: does it seal or not?

All of the above algorithms need to be calibrated in some way because the resultant numbers are not, in themselves, a prediction of seal capacity. The simplest kind of calibration looks for a threshold

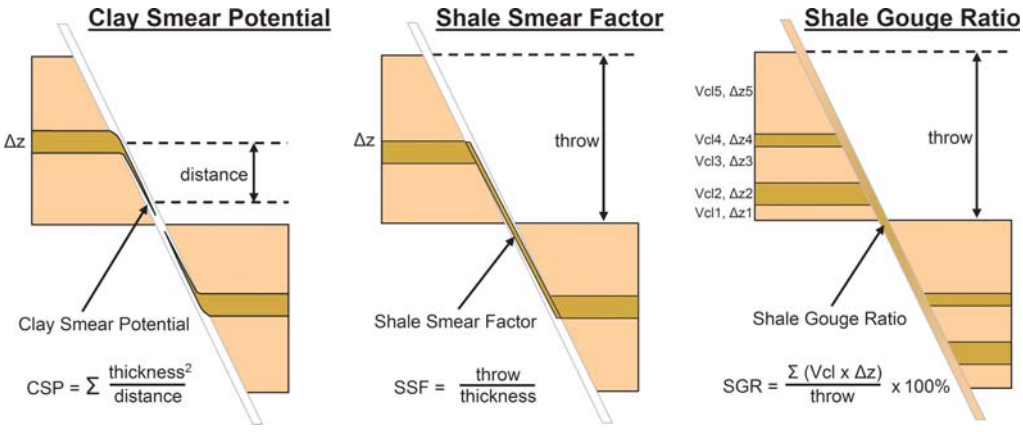

Fig. 3. The three main fault-seal algorithms. After Yielding *et al.* (1997), redrawn by Jolley *et al.* (2007).

number which separates sealing locations from non-sealing locations on the fault surface (or strictly, probably sealing from probably non-sealing).

Figure 5 gives some examples of calibration of Shale Smear Factor (SSF) based on lab experiments and outcrop observations. The property that is measured here is the continuity of the smear from upthrown to downthrown side, as seen in a cross-section view. When SSF is small, all smears are continuous; when SSF is large, all smears ultimately become discontinuous. The assumption is that a continuous smear can act as a seal whereas a discontinuous smear will not (and no other sealing fault rocks are present). From the shape of the curves, one might conclude that when SSF $<4-5$ there is a high chance of a continuous smear (and therefore the presence of seal at the fault). Færseth (2006) suggests a critical SSF of ≤ 4 from a study of larger faults at outcrop. To apply this critical value to subsurface prediction, a further assumption must be made that along-strike variation would not change the cross-section statistics shown in Figure 5.

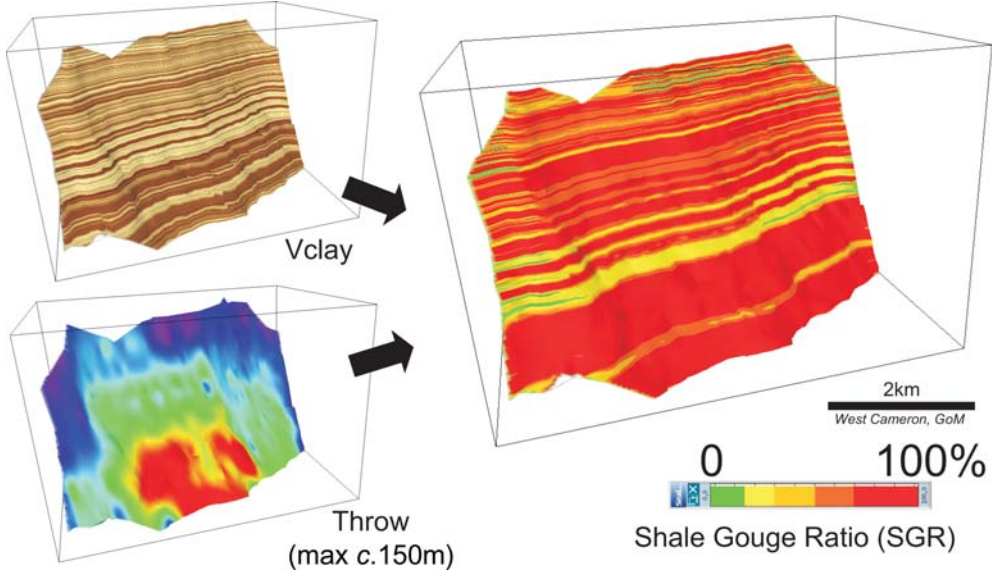

Fig. 4. Example of a subsurface fault-seal model. The fault surface was interpreted on 3D seismic reflection data (West Cameron area, Gulf of Mexico). Upper left diagram shows the sand-shale pattern mapped onto the upthrown side of the fault from well curves (Vshale). Lower left diagram shows the displacement pattern mapped on the fault surface (from horizon offsets). Right diagram shows calculated distribution of shale gouge ratio (SGR) (equation in Fig. 3).

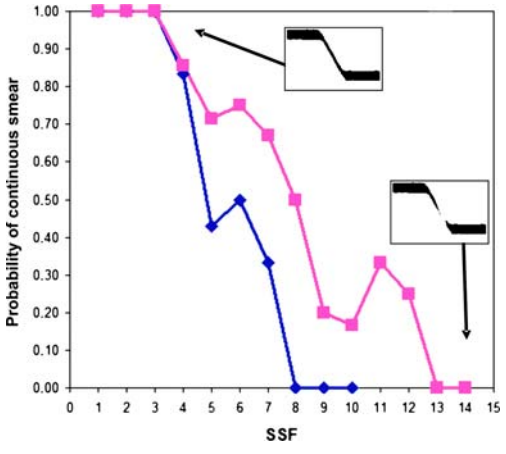

Fig. 5. Two calibrations of Shale Smear Factor (SSF). The curves show the observed probability of a smear being continuous from upthrown to downthrown side in cross-section view, at various different values of SSF (throw/thickness, Fig. 3). The blue curve summarizes deformation of laboratory samples (Takahashi 2003); the magenta curve summarizes outcrop observations by Childs *et al.* (2007).

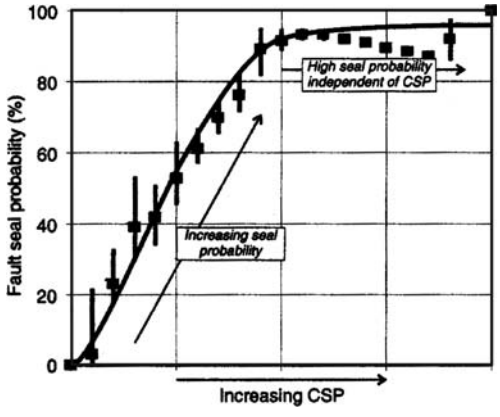

Fig. 6. Subsurface calibration of Clay Smear Potential (CSP) published by Fulljames *et al.* (1997). The data for this calibration were gathered on 91 reservoirs along 10 faults in three different fields (Niger Delta). (No scale on horizontal axis in original figure.)

To calibrate the attribute more directly, it is better to use calculations on mapped subsurface faults that are known from well data to be sealing. Figure 6 shows a calibration of Clay Smear Potential (CSP) using subsurface fault mapping in Shell's Niger Delta fields (from Fulljames *et al.* 1997). At low CSP very few reservoir–reservoir juxtapositions are observed to seal, but the proportion of sealing juxtapositions progressively rises as CSP increases, up to a 'saturation' value after which the seal probability does not increase further. Unfortunately the calibration was published without numbers on the CSP axis. Jev *et al.* (1993) state that in another nearby field, CSP > 30 represents a sealing value.

A similar subsurface calibration is shown in Figure 7 for SGR. The two curves, representing observations from the Columbus Basin and the Brent Province, imply that when SGR $> c.$ 20% there is a high chance of a fault-zone seal. Both these examples are from sand-shale sequences where the smear-free parts of the fault zones are composed of non-sealing disaggregation-zones (as seen in well cores, e.g. Fisher & Knipe 2001). The correspondence between this SGR threshold of 20%, and the maximum clay content of disaggregation zones (20%) gives some credence to the assumption that the SGR value is representing the fault-zone composition.

All of the calibrations shown in Figures 5–7 relate to geological environments where seal at the fault surface is developed by clay/shale smear or phyllosilicate-framework fault rock, and where clay-poor fault rock is disaggregation zone rather than cataclasite. The threshold value of the fault-seal attribute can therefore be viewed as an on/off switch between non-sealing areas (disaggregation zones) and well-sealed areas (smears, PFFR). In many exploration contexts, this may be sufficient to test the viability of a fault-bound prospect. However, often a more quantitative result will be needed – specifically, how tall a hydrocarbon column might the fault seal hold back? Also, in cases where cataclasites or cemented fault rocks are present, the non-smeared parts of a fault plane may also seal. The next section reviews calibrations for these situations.

Calibration: how much does the seal hold?

Over the last two decades, two fundamentally different approaches have been advocated to predict the capacity of fault seals. These approaches have often been referred to as deterministic and empirical.

- *Deterministic approach*. Values of capillary threshold pressure and clay content are measured in the lab for fault rock samples local to the prospect (e.g. from nearby cored wells). To assign these various measurements to the appropriate reservoir-reservoir juxtapositions, it is usually necessary to perform an SGR analysis of the fault and then (assuming that SGR equals the clay content of the fault-zone) the measured capillary threshold values can be interpolated onto the fault.
- *Empirical approach*. SGR analysis is performed on known sealing faults, and compared with

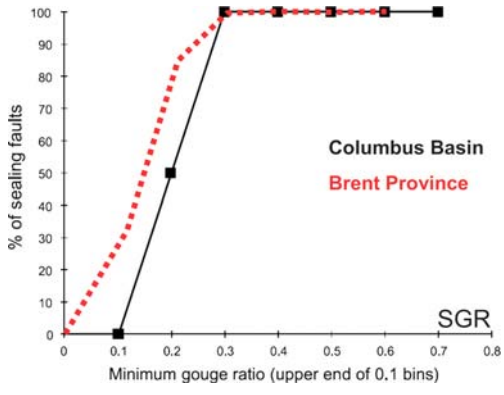

Fig. 7. Two subsurface calibrations of Shale Gouge Ratio. Black line summarizes calibration data from 12 reservoirs along 7 faults in Mahogany field, Columbus Basin, offshore Trinidad (from Gibson & Bentham 2003). Red line summarizes data from 29 faults in 15 fields in the Brent Province (from Yielding 2002).

measured hydrocarbon column heights or pressure differences trapped at the fault. The derived SGR – column height relationship is then used predictively on adjacent prospects. Note that SGR is used as a proxy attribute to obtain seal capacity – this approach does not require that SGR corresponds to any real geological property.

The deterministic approach is perhaps best exemplified by the work of Sperrevik *et al.* (2002). Measurements of permeability and Hg–air capillary threshold pressure were made on core samples of microfaults from nine fields in the northern North Sea and mid-Norway shelf. (Fault displacements were in the range millimetres to centimetres.) Results were analysed in terms of fault clay content, depth at time of faulting, and maximum burial depth – these are the three controlling factors described above in the section on Fault-zone processes. Best-fit polynomial equations were derived to express the variation in permeability and threshold pressure in terms of these three variables. Examples of subsets of the database are shown in Figure 8. Threshold pressures increase with fault-zone clay content and with maximum burial depth, and at low clay contents they also increase with depth of burial during faulting (cataclasis effect). Assuming that subsurface fault rock clay content is given by SGR, and that the faulting/burial history is known, then the derived equations can be used for prediction of subsurface fault-seal capacity. Because the equations are a best-fit through a scatter of measured capillary pressures, they can be regarded as an *average* prediction of fault rock seal capacity for a given set of input variables.

Two significant issues can be raised with regard to the deterministic approach. Firstly, the measurements of fault rock properties are made on plug samples from microfaults with mm–cm displacements. Such small faults are relatively simple and do not have the complex internal structure of trap-bounding faults with >10 m displacement (e.g. Childs *et al.* 1997; Foxford *et al.* 1998; Wibberley *et al.* 2008). Larger faults typically comprise multiple components (e.g. smears, clay-poor fault rock, and intact protolith), rather than uniformly mixed material. It is arguable whether SGR gives a representative estimate of fault-zone composition – within the upscaled 'average', there are always likely to be smear components that are relatively more sealing. We return to this point later.

A second issue is that lab-measured capillary threshold pressures are obtained in the mercury-air system, whereas obviously the relevant system for fault-seal prediction is hydrocarbon–water. Hg–air values can be converted to hydrocarbon-water values if the interfacial tension for the hydrocarbon-water system is known for the subsurface PT conditions. This information is frequently unknown. Values are known to depend upon fluid type, temperature and pressure, as indicated in Figure 9. At shallow depths the variation with fluid type is considerable, though appears to reduce with increasing depth. Because the Hg–air interfacial tension is much higher than the hydrocarbon–water values shown in Figure 9, hydrocarbon–water threshold pressures will be smaller than measured Hg–air threshold pressures by a factor of 0.08–0.16 depending on hydrocarbon type and PT conditions, giving a factor of 2 range in the final result.

The empirical approach to calibration involves studying a known sealing fault and computing the pressure difference across it at each reservoir–reservoir juxtaposition. Comparison with a fault-seal attribute (such as shale gouge ratio) at the same points on the fault can reveal whether there is any relationship between the attribute and the supported pressure difference, see Figure 10. This workflow was introduced by Yielding *et al.* (1997), and additional examples were compiled and summarized by Yielding (2002) and Bretan *et al.* (2003). Although a local calibration is always preferred for predictive purposes (to ensure cases with the same geological history), it is instructive to combine different datasets to reveal broader trends in the relationships. Figure 10 shows a global compilation of data from many basins (see figure caption for details), and indicates a general trend of increasing SGR value being able to support increasing across-fault pressure difference (AFPD). Lines represent 'seal-failure envelopes', that is, maximum across-fault pressure that can be supported at a specific SGR value, for particular maximum burial

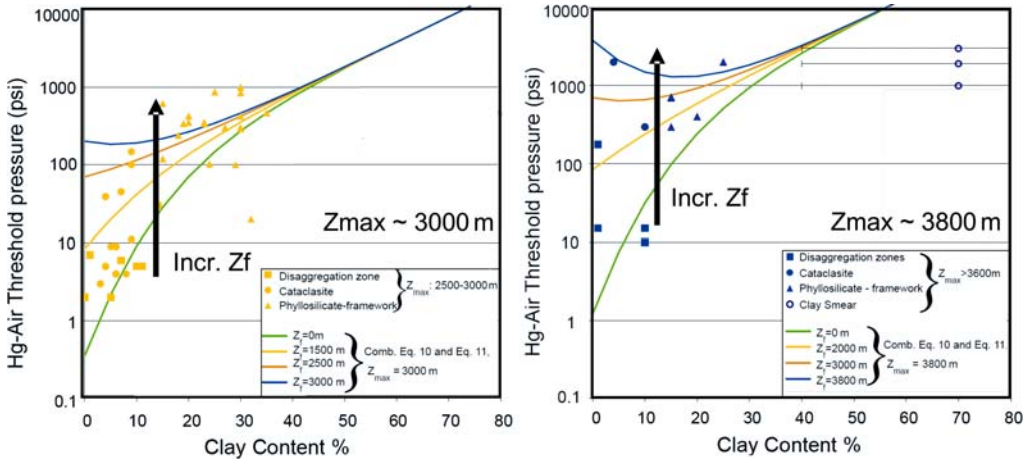

Fig. 8. Examples of laboratory measurements of Hg–Air threshold pressure of fault rock samples from the northern North Sea (Sperrevik *et al.* 2002). Diagram at left presents measurements on samples buried to 2500–3000 m, whereas that at right shows measurements on samples buried >3600 m. The curves are examples of a model equation fitted to >100 samples, which relates threshold pressure to variations in fault rock clay content, maximum burial depth Zmax, and depth of burial at time of faulting Zf.

depths. Note that the seal-failure envelope for shallow depths (<3 km, blue) exhibits no seal at SGR < 15–20%, corresponding to the simple seal/no-seal threshold discussed in the previous section. Because the envelopes are drawn along the upper edge of all observed data, they represent a *maximum* seal capacity for any combination of input data – contrast with the equations based on fault rock sample measurements, which represent an *average* seal capacity at given conditions.

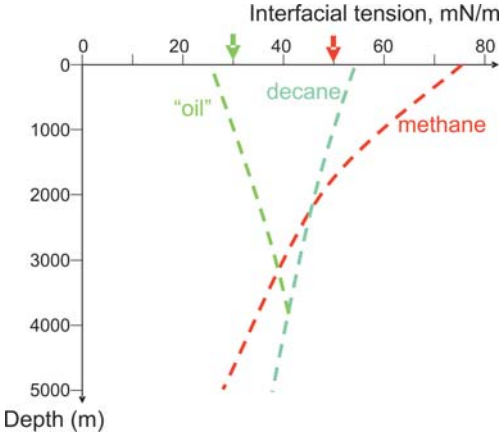

Fig. 9. Some published estimates of the variation of hydrocarbon–water interfacial tension with respect to depth (pressure & temperature conditions). The methane & decane curves indicate experimentally-measured trends from Firoozabadi & Ramey (1988). The 'oil' values are from Nordgård Bolås *et al.* (2005), constructed from empirical equations of Firoozabadi & Ramey (1988). Arrows show typical industry default values for oil–water (green) and gas–water (red) (d'Onfro, pers. comm., 2007).

Some of the original data included in the Figure 10 compilation involved across-fault aquifer changes (Bretan *et al.* 2003). These are not relevant as examples of static capillary trapping, which by definition is a physical process dependent on the presence of two immiscible phases. Figure 11 (left) is a revised compilation, concentrating on true buoyancy pressures measured in the hydrocarbon phase relative to the aquifer pressure at the fault. If aquifer pressures are the same across the fault, then this is a measure of the buoyancy pressure in the trap relative to the water in the fault rock (the sealing lithology). On the other hand, if aquifer pressures differ across the fault, then the plotted buoyancy pressure is the difference between the hydrocarbon phase and the *higher*-pressure aquifer (see discussion by Underschultz 2007). Cases where the across-fault pressure differences are measured between different aquifers (no hydrocarbon involved) have been omitted. Such data are telling us about the hydrodynamic behaviour of the fault rather than its static trapping capacity (e.g. Grauls *et al.* 2002; Harris *et al.* 2002). This is an important distinction: in hydrodynamic systems the pressure drop between aquifers at the fault will depend upon the fault rock permeability and thickness (not threshold pressure) and the overall flow rate.

In Figure 11 (left) the dashed lines show a possible revision of the seal-failure envelopes for depths <3 km (blue) and >3.5 km (green). Compared with

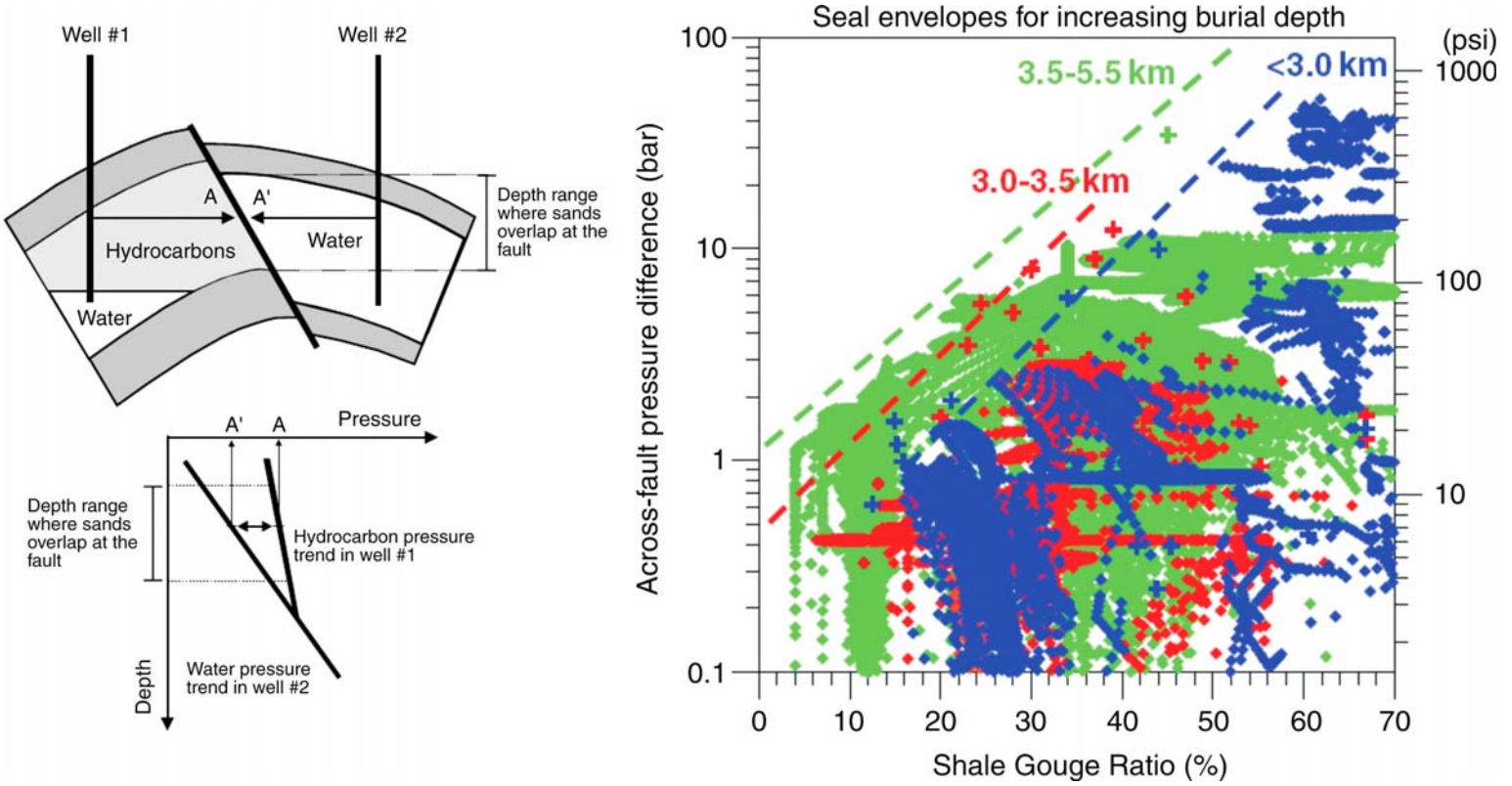

Fig. 10. The empirical approach to faul-seal calibration (from Bretan *et al.* 2003). The insets at left show how the across-fault pressure difference can be defined at reservoir-reservoir overlaps from data at adjacent wells. The plot at right shows a global compilation of across-fault pressure differences and their relationship to SGR at the same point on the fault surface. Data come from several tens of faults in nine different extensional basins. Clouds of small points correspond to entire reservoir juxtaposition areas. Large points (+) correspond to 'trap-critical' locations that represent the highest pressure difference at a particular value of SGR on that fault. Data points are coloured by maximum burial depth, blue <3 km, red 3–3.5 km, green >3.5 km. The dashed lines indicate suggested log-linear fault-seal-failure envelopes for the different depth ranges.

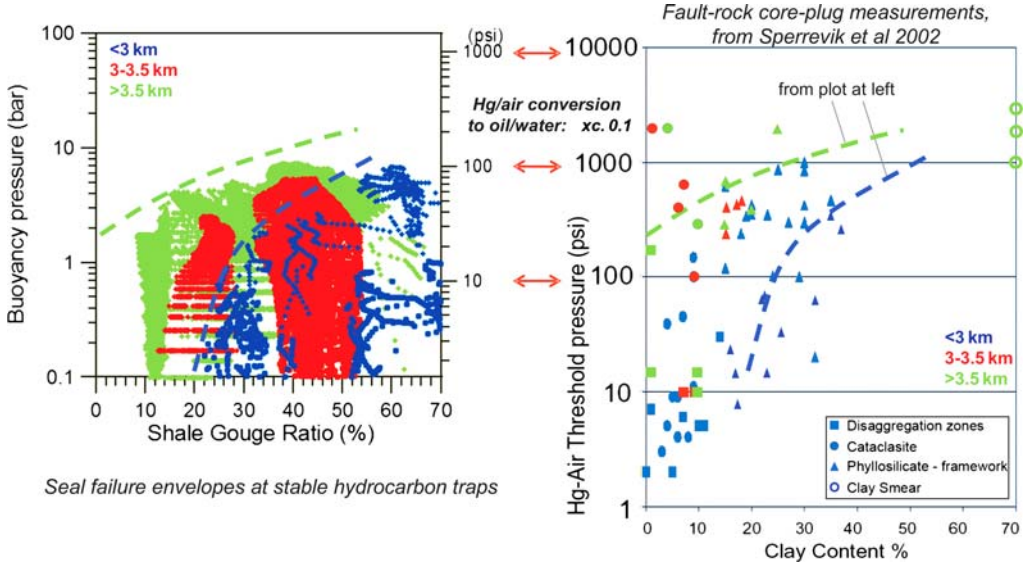

Fig. 11. A comparison of deterministic (lab) measurements and empirical calibration of seal capacity as a function of fault rock composition or shale gouge ratio. The cross-plot at left is subset of the subsurface data presented in Figure 10, filtered to retain only true measurements of hydrocarbon buoyancy pressure (Bretan & Yielding 2005; Underschultz 2007). Data points are coloured by maximum burial depth, blue <3 km, red 3–3.5 km, green >3.5 km. The cross-plot at right is an example of Hg–air core-plug threshold pressures from Sperrevik *et al.* (2002). The vertical axes of the two plots are aligned assuming that hydrocarbon/water threshold pressures are one tenth of the Hg–air values. The curved lines are possible fault-seal failure envelopes, constructed on the plot of subsurface data (left) but also drawn on the core-plug data (right) – note the consistency of the two approaches.

Figure 10, some of higher pressure differences at high SGR are removed. The data now do not justify a continued increase in trapping potential above about 40–50% SGR. A possible interpretation is that sealing by clay smears becomes complete over the fault surface at this value, and addition of further clay smear does not enhance the capillary sealing capacity (in the same way that doubling the thickness of a top seal layer does not double its sealing capacity).

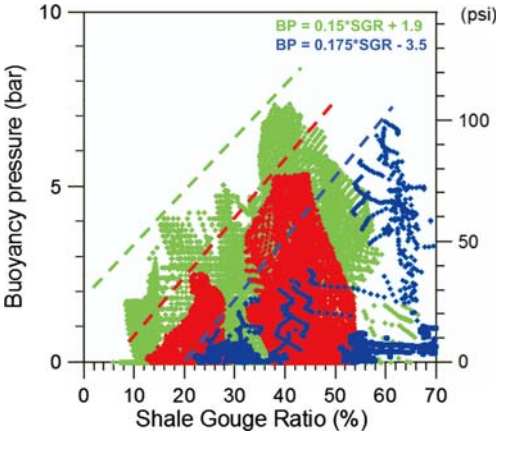

Fig. 12. Linear plot of the same data as that shown in the left-hand plot of Figure 11. Data points are coloured by maximum burial depth, blue <3 km, red 3–3.5 km, green >3.5 km. Note that linear seal-failure envelopes are consistent with the data distribution.

Also shown in Figure 11 (at right) is an example of the deterministic calibration of Sperrevik *et al.* (2002); a factor of ×0.1 aligns the vertical axes of the two plots, on the assumption that hydrocarbon–water threshold pressures are about one tenth of Hg–air values. The revised seal-failure envelopes from the subsurface plot (at left of figure) are also shown on this plot for reference. It is striking, and perhaps surprising given the earlier discussion, that the subsurface seal-failure lines are broadly consistent with the core-plug measurements. The core-plug measurements display a wide scatter (order-of-magnitude), and if this variability occurs on a subsurface fault then some of the lower threshold-pressure values might be expected to be critical in controlling a particular trap fill. However, the fact that both data types suggest similar trends for fault-zone threshold pressures gives some support to the use of SGR as a proxy for average fault-zone clay content – even though

large trap-bounding faults are expected to be more heterogeneous. This is an important result, and indicates that (for practical purposes) estimates of fault-seal capacity produced by the empirical and deterministic methodologies are not mutually exclusive but rather are alternative possibilities in the range of subsurface uncertainty.

The revised empirical seal-failure envelopes shown on Figure 11 are curved, which suggests that a log-linear relationship is not the most appropriate. Figure 12 shows the same data as Figure 11, but plotted with linear axes instead of log-linear. This revised compilation is perhaps better described by linear fault-seal failure envelopes, more similar to those originally suggested in the initial application of this methodology (Yielding *et al.* 1997). Addition of further datasets in the future will doubtless continue to revise these bounding envelopes.

The most promising future avenue for quantifying seal-prediction uncertainty appears to be a greater understanding of fault-zone heterogeneity, particularly at intermediate clay-contents. At high clay content (high SGR, e.g. >50%), both methodologies would interpret the fault rock as being dominated by clay smear, and therefore the capillary properties of clay smears should be representative of the fault surface. At low clay content (low SGR, <20%), the fault rock is likely to be dominated by disaggregation zones or cataclasites, and again the properties of these rocks are likely to be appropriate for the fault surface. However, at intermediate SGR values (20–50%) differing interpretations are possible: the deterministic approach would infer that the fault-zone is composed of phyllosilicate-framework fault rocks (PFFR) like those sampled in core-plugs of microfaults, whereas the empirical approach simply uses observed in-situ pressures without necessarily requiring a particular fault rock composition. Observations of large faults at outcrop would generally reveal a heterogeneous assemblage of clay-poor components and clay/shale smears (some possibly discontinuous) rather than a slab of PFFR. So, although the average or upscaled composition of the fault zone may be the same as a PFFR, PFFRs might be only a minor component: the assemblage of smears may provide the control on the fault-zone properties.

Interestingly, Childs *et al.* (2007) have produced stochastic models of disrupted impermeable shale smears and then examined the effective fault-zone permeabilities that result. When fault throws are much greater than the bed thicknesses, the effective permeability of the fault zone is equivalent to a simple log-linear relationship between SGR and permeability, mimicking the observed log-linear relationship between fault rock clay content and permeability (Sperrevik *et al.* 2002). This result cannot be directly applied to threshold pressures, since trapping does not depend on average properties and one weak spot could destroy the seal. However, modelling of trapped column heights (as opposed to threshold pressure) relative to disrupted shale smear geometries suggests that an analogous relationship can arise, with taller columns being trapped as more disrupted smears are entrained in the fault zone (Yielding 2009) If confirmed, this would imply that the apparent consistency of the empirical and deterministic approaches at intermediate SGR values is largely coincidental, and improving the agreement by further work should not be expected.

Conclusions

- Fault seal algorithms are required to characterize variation over a mapped subsurface fault.
- Each algorithm needs to be calibrated against local data to be meaningful.
- Calibration may be qualitative (on/off) or quantitative (pressure differences or column heights).
- Published calibrations have involved fault-zone samples in the lab ('deterministic'), or hydrocarbon traps in the subsurface ('empirical').
- Surprisingly, lab & in-situ calibrations often agree to within a factor of 2–3. Comparison of the two approaches is perhaps one estimate of the uncertainty in any prediction, given the influence of fault zone heterogeneity on fluid trapping processes. Further outcrop studies of larger (trap-bounding scale) faults may represent the best way to quantify this uncertainty.

Many thanks to reviewers Chris Wibberley and Pete D'Onfro for suggestions that improved an earlier version of this manuscript. Conrad Childs is thanked for providing a copy of his Shale Smear modelling paper. Discussions with Quentin Fisher are gratefully acknowledged.

References

Allan, U. S. 1989. Model for hydrocarbon migration and entrapment within faulted structures. *American Association of Petroleum Geologists Bulletin*, **73**, 803–811.

Aydin, A. & Eyal, Y. 2002. Anatomy of a normal fault with shale smear: implications for fault seal. *American Association of Petroleum Geologists Bulletin*, **86**, 1367–1381.

Barton, C. A., Zoback, M. D. & Moos, D. 1995. Fluid flow along potentially active faults in crystalline rock. *Geology*, **23**, 683–686.

Bouvier, J. D., Kaars-Sijpesteijn, C. H., Kluesner, D. F., Onyejekwe, C. C. & Van der Pal, R. C. 1989. Three-dimensional seismic interpretation and fault sealing investigations, nun river field, Nigeria.

American Association of Petroleum Geologists Bulletin, **73**, 1397–1414.

BRETAN, P. & YIELDING, G. 2005. Using buoyancy pressure profiles to assess uncertainty in fault seal calibration. *In*: BOULT, P. & KALDI, J. (eds) *Evaluating Fault and Cap Rock Seals*. American Association of Petroleum Geologists Hedberg Series, Tulsa, **2**, 151–162.

BRETAN, P., YIELDING, G. & JONES, H. 2003. Using calibrated shale gouge ratio to estimate hydrocarbon column heights. *American Association of Petroleum Geologists Bulletin*, **87**, 397–413.

CHILDS, C., WATTERSON, J. & WALSH, J. J. 1996. A model for the structure and development of fault zones. *Journal of the Geological Society, London*, **153**, 337–340.

CHILDS, C., WATTERSON, J. & WALSH, J. J. 1997. Complexity in fault zone structure and implications for fault seal prediction. *In*: MØLLER-PEDERSEN, P. & KOESTLER, A. G. (eds) *Hydrocarbon Seals: Importance for Exploration and Production*, Norwegian Petroleum Society (NPF) Special Publication, Elsevier Science, Singapore, **7**, 61–72.

CHILDS, C., WALSH, J. J. *ET AL*. 2007. Definition of a fault permeability predictor from outcrop studies of a faulted turbidite sequence, Taranaki, New Zealand. *In*: JOLLEY, S. J., BARR, D., WALSH, J. J. & KNIPE, R. J. (eds) *Structurally Complex Reservoirs*. Geological Society, London, Special Publications, **292**, 235–258.

DEE, S., FREEMAN, B., YIELDING, G., ROBERTS, A. & BRETAN, P. 2005. Best practice in structural geological analysis. *First Break*, **23**, 49–54.

DOUGHTY, P. T. 2003. Clay smear seals and fault sealing potential of an exhumed growth fault, Rio Grande rift, New Mexico. *American Association of Petroleum Geologists Bulletin*, **87**, 427–444.

EICHHUBL, P., D'ONFRO, P. S., AYDIN, A., WATERS, J. & MCCARTY, D. K. 2005. Structure, petrophysics, and diagenesis of shale entrained along a normal fault at black diamond mines, California – implications for fault seal. *American Association of Petroleum Geologists Bulletin*, **89**, 1113–1137.

FÆRSETH, R. B. 2006. Shale smear along large faults: continuity of smear and the fault seal capacity. *Journal of Geological Society, London*, **163**, 741–752.

FIROOZABADI, A. & RAMEY, H. J. 1988. Surface tension of a water hydrocarbon system at reservoir conditions. *Journal of Canadian Petroleum Technology*, **27**, 3.

FISHER, Q. J. & KNIPE, R. J. 1998. Fault sealing processes in siliciclastic sediments. *In*: JONES, G., FISHER, Q. J. & KNIPE, R. J. (eds) *Faulting, Fault Sealing and Fluid Flow in Hydrocarbon Reservoirs*. Geological Society, London, Special Publications, **147**, 117–134.

FISHER, Q. J. & KNIPE, R. J. 2001. The permeability of faults within siliciclastic petroleum reservoirs of the North Sea and Norwegian Continental Shelf. *Marine & Petroleum Geology*, **18**, 1063–1081.

FISHER, Q. J., CASEY, N., HARRIS, S. D. & KNIPE, R. J. 2003. Fluid-flow properties of faults in sandstone: the importance of temperature history. *Geology*, **31**, 965–968.

FOSSEN, H. & GABRIELSEN, R. H. 2005. *Strukturgeologi*. Fagbokforlaget, Bergen, Norway, 1–369.

FOSSEN, H., SCHULTZ, R. A., SHIPTON, Z. K. & MAIR, K. 2007. Deformation bands in sandstone: a review. *Journal of Geological Society, London*, **164**, 755–769.

FOXFORD, K. A., WALSH, J. J., WATTERSON, J., GARDEN, I. R., GUSCOTT, S. C. & BURLEY, S. D. 1998. Structure and content of the Moab Fault Zone, Utah, USA, and its implications for fault seal prediction. *In*: JONES, G., FISHER, Q. J. & KNIPE, R. J. (eds) *Faulting, Fault Sealing and Fluid Flow in Hydrocarbon Reservoirs*. Geological Society, London, Special Publications, **147**, 87–103.

FREEMAN, B., YIELDING, G., NEEDHAM, D. T. & BADLEY, M. E. 1998. Fault seal prediction: the gouge ratio method. *In*: COWARD, M. P., DALTABAN, T. S. & JOHNSON, H. (eds) *Structural Geology in Reservoir Characterization*. Geological Society, London, Special Publications, **127**, 19–25.

FRISTAD, T., GROTH, A., YIELDING, G. & FREEMAN, B. 1997. Quantitative fault seal prediction: a case study from Oseberg Syd. *In*: MØLLER-PEDERSEN, P. & KOESTLER, A. G. (eds) *Hydrocarbon Seals: Importance for Exploration And Production*. Norwegian Petroleum Society (NPF) Special Publication, Elsevier Science, Singapore, **7**, 107–124.

FULLJAMES, J. R., ZIJERVELD, L. J. J. & FRANSSEN, R. C. M. W. 1997. Fault seal processes: systematic analyses of fault seals over geological and production time scales. *In*: MØLLER-PEDERSEN, P. & KOESTLER, A. G. (eds) *Hydrocarbon Seals: Importance for Exploration and Production*. Norwegian Petroleum Society (NPF) Special Publication, Elsevier Science, Singapore, **7**, 51–59.

GIBSON, R. G. 1998. Physical character and fluid-flow properties of sandstone-derived fault gouge. *In*: COWARD, M. P., DALTABAN, T. S. & JOHNSON, H. (eds) *Structural Geology in Reservoir Characterization*. Geological Society, London, Special Publications, **127**, 83–97.

GIBSON, R. G. & BENTHAM, P. A. 2003. Use of fault-seal analysis in understanding petroleum migration in a complexly faulted anticlinal trap, Columbus Basin, offshore Trinidad. *American Association of Petroleum Geologists Bulletin*, **87**, 465–478.

GRAULS, D., PASCAUD, F. & RIVES, T. 2002. Quantitative fault seal assessment in hydrocarbon-compartmentalised structures using fluid pressure data. *In*: KOESTLER, A. G. & HUNSDALE, R. (eds) *Hydrocarbon Seal Quantification*. Norwegian Petroleum Society (NPF) Special Publication, Amsterdam, **11**, 141–156.

HARRIS, D., YIELDING, G., LEVINE, P., MAXWELL, G., ROSE, P. T. & NELL, P. 2002. Using Shale Gouge Ratio (SGR) to model faults as transmissibility barriers in reservoirs: an example from the Strathspey field, North Sea. *Petroleum Geoscience*, **8**, 167–176.

JEV, B. I., KAARS-SIJPERSTEIJN, C. H., PETERS, M. P. A. M., WATTS, N. L. & WILKIE, J. T. 1993. Akaso Field, Nigeria: use of integrate 3D seismic, fault-slicing, clay smearing and RFT pressure data on fault trapping and dynamic leakage. *American Association of Petroleum Geologists Bulletin*, **77**, 1389–1404.

JOLLEY, S. J., DIJK, H., LAMENS, J. H., FISHER, Q. J., MANZOCCHI, T., EIKMANS, H. & HUANG, Y. 2007. Faulting and fault sealing in production simulation models: Brent province, northern North Sea. *Petroleum Geoscience*, **13**, 321–340.

JONES, R. M. & HILLIS, R. R. 2003. An integrated, quantitative approach to assessing fault-seal risk. *American Association of Petroleum Geologists Bulletin*, **87**, 507–524.

LEHNER, F. K. & PILAAR, W. F. 1997. The emplacement of clay smears in synsedimentary normal faults: inferences from field observations near Frechen, Germany. *In*: MØLLER-PEDERSEN, P. & KOESTLER, A. G. (eds) *Hydrocarbon Seals: Importance for Exploration and Production*. Norwegian Petroleum Society (NPF) Special Publication, Elsevier Science, Singapore, **7**, 39–50.

LINDSAY, N. G., MURPHY, F. C., WALSH, J. J. & WATTERSON, J. 1993. Outcrop studies of shale smear on fault surfaces. *In*: FLINT, S. & BRYANT, A. D. (eds) *The Geological Modelling of Hydrocarbon Reservoirs and Outcrop*. Special Publication International Association of Sedimentologists, Blackwell, Oxford, **15**, 113–123.

NORDGÅRD BOLÅS, H. M., HERMANRUD, C. & TEIGE, G. M. G. 2005. Seal capacity estimation from subsurface pore pressures. *Basin Research*, **17**, 583–599.

OXFORD PAPERBACK DICTIONARY. 1988. 3rd edn. Oxford University Press, Oxford.

SPERREVIK, S., GILLESPIE, P. A., FISHER, Q. J., HALVORSEN, T. & KNIPE, R. J. 2002. Empirical estimation of fault rock properties. *In*: KOESTLER, A. G. & HUNSDALE, R. (eds) *Hydrocarbon Seal Quantification*. Norwegian Petroleum Society (NPF) Special Publication, Amsterdam, **11**, 109–125.

TAKAHASHI, M. 2003. Permeability change during experimental fault smearing. *Journal of Geophysical Research*, **108**, B5.

TEARPOCK, D. J. & BISHKE, R. E. 2003. *Applied Subsurface Geological Mapping*. 2nd edn. Prentice Hall PTR, New Jersey, 1–822.

UNDERSCHULTZ, J. 2007. Hydrodynamics and membrane seal capacity. *Geofluids*, **7**, 148–158.

VAN DER ZEE, W. & URAI, J. L. 2005. Processes of fault evolution in a siliciclastic sequence: a case study from Miri, Sarawak, Malaysia. *Journal of Structural Geology*, **27**, 2281–2300.

WEBER, K. J., MANDL, G., PILAAR, W. F., LEHNER, F. & PRECIOUS, R. G. 1978. The role of faults in hydrocarbon migration and trapping in Nigerian growth fault structures. *10th Annual Offshore Technology Conference Proceedings*, **4**, 2643–2653.

WIBBERLEY, C. A. J., YIELDING, G. & DI TORO, G. 2008. Recent advances in the understanding of fault zone internal structure: a review. *In*: WIBBERLEY, C. A. J., KURTZ, W., IMBER, J., HOLDSWORTH, R. E. & COLLETTINI, C. (eds) *The Internal Structure of Fault Zones: Implications for Mechanical and Fluid-Flow Properties*. Geological Society, London, Special Publications, **299**, 5–33.

YIELDING, G. 2002. Shale Gouge Ratio – calibration by geohistory. *In*: KOESTLER, A. G. & HUNSDALE, R. (eds) *Hydrocarbon Seal Quantification*. Norwegian Petroleum Society (NPF) Special Publications, Amsterdam, **11**, 1–15.

YIELDING, G. 2009. Using Probabilistic Shale Smear Factor to relate SGR predictions of column height to fault-zone heterogeneity. *In*: LIGTENBERG, H. & KNIPE, R. (eds) *Fault and Top Seals: from Pore to Basin Scale*. European Association of Geoscientists & Engineers (EAGE), 21–24 September 2009, Montpellier. EAGE, Houten. Paper E05, 93–95.

YIELDING, G., FREEMAN, B. & NEEDHAM, T. 1997. Quantitative fault seal prediction. *American Association of Petroleum Geologists Bulletin*, **81**, 897–917.